The Effects of Replacing Sst2 with the Heterologous RGS4 on Polarization and Mating in Yeast

Hiromasa Tanaka[†‡] and Tau-Mu Yi[†‡*]
[†]Department of Developmental and Cell Biology and [‡]Center for Complex Biological Systems, University of California, Irvine, California

ABSTRACT RGS proteins stimulate the deactivation of heterotrimeric G-proteins. The yeast RGS protein Sst2 is regulated at both the transcriptional and posttranscriptional levels. We replaced the *SST2* gene with the distantly related human *RGS4* gene, which consists of the catalytic domain and an N-terminal membrane attachment peptide, and replaced the native promoter (P_{SST2}) with the heterologous tetracycline-repressible promoter (P_{TET}). We then measured the effect of the substitutions on pheromone sensitivity, mating, and polarization. Although the pheromone sensitivity was essentially normal, there were differences in mating and polarization. In particular, the *RGS4*-substituted strains did not form multiple mating projections at high levels of α-factor, but instead formed a single malformed projection, which frequently gave rise to a bud. We provide evidence that this phenotype arose because unlike Sst2, RGS4 did not localize to the projection. We use mathematical modeling to argue that localization of Sst2 to the projection prevents excess G-protein activation during the pheromone response. In addition, modeling and experiments demonstrate that the dose of Sst2 influences the frequency of mating projection formation.

INTRODUCTION

Heterotrimeric G-proteins are activated by G-protein-coupled receptors (GPCRs) and deactivated by the regulator of G-protein signaling (RGS) proteins, and both are regulated in a spatiotemporal manner. Because of the complexity of G-protein signaling, it is important to develop more accurate mathematical models of this system (1–3).

The yeast mating response is one of the best characterized G-protein signaling systems (4–6). During mating, haploid **a** and α cells secrete and respond to the pheromones (**a**-factor and α-factor) from their partners by creating mating projections that fuse. In **a**-cells, the GPCR Ste2 binds α-factor and activates the heterotrimeric G-protein cycle, which leads to dissociation of the GTP-bound Gα-protein (Gpa1-GTP) and the G$\beta\gamma$ protein complex (Ste4/Ste18). Free G$\beta\gamma$ induces pheromone-responsive genes such as *FUS1* via the mitogen-activated protein kinase (MAPK) cascade and the transcription factor Ste12 (Fig. S1 in the Supporting Material). In addition, the activation of the G-protein cycle causes cell-cycle arrest and formation of the mating projection.

Sst2 was the first RGS protein identified (7). Sst2 deactivates the G-protein cycle by catalyzing the hydrolysis of Gpa1-GTP to Gpa1-GDP (8). Genetic disruption of the *SST2* gene causes supersensitivity to pheromones, loss of adaptation, and mating defects (9,10). Many studies have addressed the question of how Sst2 is regulated, and several mechanisms have been described, such as regulation of transcription (11), phosphorylation (12,13), endoproteolytic processing (14), and binding of regulatory proteins (15,16).

Expression of mammalian RGS proteins in yeast has been shown to downregulate pheromone signaling (17,18). These studies suggest that RGS proteins have similar biological roles in mammals and in yeast. In particular, Linder and colleagues (19) showed that the human RGS4 protein functions in yeast, and that this activity depends on the membrane localization of the protein conferred by a putative N-terminal helix.

When yeast **a**-cells are exposed continuously to high concentrations of α-factor, they will form multiple mating projections in a sequential manner (20–22). The mechanisms underlying this process are not fully understood. The seminal work of Hilloti et al. (22) was the first to demonstrate the oscillatory dynamics arising from MAPK signaling and pheromone-dependent gene expression in the yeast pheromone system, as well as the connection between these dynamics and the formation of multiple mating projections. These observations were a crucial starting point for this research.

Here, we investigated the yeast mating response quantitatively after replacing elements of the *SST2* gene with heterologous components: the tetracycline-regulatable (P_{TET}) promoter and the *RGS4* coding region. We performed halo and mating assays, and monitored pheromone-inducible transcription and morphological changes. It is interesting to note that RGS4 complemented the supersensitive phenotype of *sst2*Δ cells, but produced an unusual morphological phenotype. Our results suggest that spatial localization of the RGS functionality to the projection is important for normal morphology. Based on these data, we modeled the system, and the simulations support the hypothesis that regulation of Sst2 confers robustness on the level of G-protein signaling by preventing overactivation.

Submitted September 29, 2009, and accepted for publication April 30, 2010.

*Correspondence: tmy@uci.edu

Editor: Andre Levchenko.

0006-3495/10/08/1007/11 $2.00

doi: 10.1016/j.bpj.2010.04.078

MATERIALS AND METHODS

Strains and plasmids

Standard methods for yeast genetic and molecular biology techniques were performed (23). The strain genotypes are listed in Table S2, and descriptions of the plasmids are provided in Table S3. Most yeast strains were isogenic with RJD360, which was originally derived from the W303 background. Yeast cells were cultured in rich YPD media supplemented with adenine (YPAD) or in synthetic media (SD).

Halo assay

Halo assays of growth arrest were performed as described by Sprague in the study by Guthrie and Fink (23).

Mating assays

Quantitative mating efficiency experiments were performed as described by Hartwell (24); mating discrimination and competition assays were performed as described by Jackson and Hartwell (9).

Microscopy

To observe single cells, exponentially growing cells were treated with α-factor for the appropriate period of time (e.g., 6 h) and fixed with ice-cold formaldehyde-PBS solution (3.7% formaldehyde in PBS) for 10 min. The prepared slides were observed using a Nikon ECLIPSE TE300 inverted microscope.

Time-course experiments

Time-course experiments for FRET measurements and transcriptional activation assays using the pheromone-inducible reporter P_{FUS1}-*GFP* were performed using a Gemini XS SpectraMAX fluorometer as described previously (1).

Microfluidics experiments

We used a standard Y-chamber microfluidics device to generate the α-factor spatial gradients (25). The device was 800 μm in width and was divided into eight regions. The cells were subjected to a 0- to 100-nM α-factor gradient for 5 h, and for the directional accuracy measurements, cells located in regions 2 and 3 were assessed (~5- to ~30-nM α-factor).

Mathematical modeling

Details about the two-compartment model are found in the Supporting Material.

RESULTS

Replacing Sst2 with RGS4 and the P_{SST2} promoter with the P_{TET} promoter

The multidomain Sst2 protein possesses a C-terminal RGS (GTPase activation) domain that stimulates G-protein deactivation (Fig. 1 *A*) and an N-terminal regulatory domain termed the Mpt5-interacting (MPI) domain (15). Recent results have shown that the MPI domain contains a DEP domain responsible for binding to α-factor receptor Ste2

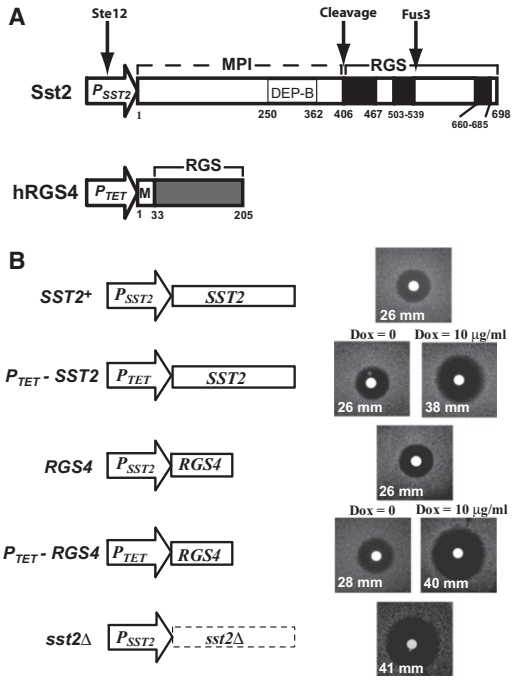

FIGURE 1 Schematic diagrams of Sst2, RGS4, and RGS constructs. (*A*) Comparison of *SST2* and *RGS4* gene structures. Sst2 is a multidomain protein in which the MPI domain is at the N-terminus and the RGS domain is at the C-terminus (amino acid positions are shown). A DEP domain that binds Ste2 lies within the MPI domain. The conserved RGS sequence blocks are shaded black. Sst2 is phosphorylated at Ser^{539} by Fus3 and is proteolytically cleaved at the boundary between the MPI and RGS domains. The P_{SST2} promoter is pheromone-inducible via the transcription factor Ste12. The human RGS4 protein contains an N-terminal membrane attachment helix (1–33, *M*), followed by the RGS domain (*gray*). (*B*) Pheromone sensitivity measured by halo assay of various RGS constructs, with 1 μg of α-factor used in assay; halos are shown at right. All constructs were integrated into the genome, e.g., the P_{TET} promoter replaced the P_{SST2} promoter, and the *RGS4* gene replaced the *SST2* gene. The constructs using the P_{TET} promoter were tested at 0 (induced) and 10 μg/ml of doxycycline (repressed), which was added to the soft agar. The average sizes (mm) of the halos for the strains are indicated.

(16). To investigate the role of the N-terminal domain, along with other potential regulatory elements, we substituted Sst2 with the human RGS4 protein (hRGS4), which consists of a minimal RGS catalytic domain attached to an N-terminal membrane-binding helix (Fig. 1 *A*) that functions in yeast (19).

In addition, to study the role of pheromone-inducible expression of *SST2*, we replaced the native *SST2* promoter with a heterologous promoter (P_{TET}) regulated by the tetracycline analog doxycycline (26). The P_{TET} promoter is active in the absence of doxycycline and is repressed by doxycycline added to the growth medium. A concentration of 10 μg/ml was sufficient to confer maximal repression with no effect on yeast mating morphology.

The halo assay is a common method for assessing pheromone signaling (23). The mating response causes cell-cycle arrest, and spotting α-factor on to a lawn of yeast cells results in a halo whose diameter is a quantitative measure

of the dose response of pheromone signaling in that strain. Note that in this study, we refer to *bar1*Δ cells as wild-type; *BAR1* encodes for a protease that degrades α-factor. Only in the mating experiments were the *MAT**a*** strains $BAR1^+$. Using 1 μg of α-factor, wild-type cells formed a halo with a diameter of 26 mm (Fig. 1 *B*). Mutant *sst2*Δ cells were supersensitive, resulting in a much larger halo (41 mm). The *RGS4* strain showed a halo size (26 mm) comparable to that of wild-type cells, confirming that RGS4 could substitute for Sst2 in terms of pheromone sensitivity measured by the halo assay (17).

In the P_{TET}-*SST2* strain without doxycycline, the halo size was comparable to that of the wild-type *SST2* strain (26 mm). In the presence of doxycycline, the halo size was slightly smaller (38 mm) than that of the *sst2*Δ strain. Thus, the range of expression from the P_{TET} system was approximately from wild-type P_{SST2} levels to slightly higher than a complete deletion. In the P_{TET}-*RGS4* strain, at the highest level of RGS4, the halo size (28 mm) was roughly the same as in the wild-type *SST2* or *RGS4* strains, whereas at the lowest level of RGS4, the halo (40 mm) was almost the same size as in the *sst2*Δ strain. These data indicate that RGS4 can confer deactivation approximately equivalent in capacity to that of Sst2 and that both function in a concentration-dependent manner.

Mating efficiency, discrimination, and competition in strains containing RGS variants

The above results showed that the native *SST2* gene could be replaced with the completely heterologous P_{TET}-*RGS4* gene construct and the resulting strain would possess approximately wild-type pheromone sensitivity evaluated by the halo assay. A more stringent test of functionality is the ability to mate, and we evaluated the RGS variants by three mating assays. First, the mating efficiency assay determined the percent of **a**-cells ($BAR1^+$) being tested that are capable of mating with an α-cell under standard mating conditions. Second, the mating discrimination assay tested the ability of a given **a**-cell to mate selectively with cells that produce α-factor over those that do not, i.e., pheromone nonproducing decoys (9). Third, the mating competition assay measured the ability of a mutant **a**-cell to compete with wild-type **a**-cells for a limiting number of α-cell mating partners. Under equal competition, the ratio of challenger **a**-cells that mate compared to wild-type cells should be 1:1. The three assays are not equivalent and may measure different aspects of mating.

As previously reported (9,28), the *sst2*Δ strain possessed significant mating defects. In our hands, mating efficiency was 28% compared to nearly 100% for $SST2^+$ cells (Table 1). In addition, *sst2*Δ cells could not discriminate between α-factor producers versus nonproducing decoys, whereas wild-type cells selectively mated with a 10^5-fold preference for α-cells making α-factor. In mating competition assays, only 9% of *sst2*Δ cells mated compared to 91% of wild-type cells. It is clear that the presence of *SST2* is crucial for optimal mating, and we wished to examine the performance of the RGS variants.

TABLE 1 Mating assays

Responder strain	Mating efficiency	Mating discrimination	Mating competition
$SST2^+$	96 ± 9%	0.0012 ± 0.0003%	ND
*sst2*Δ	28 ± 2%	38 ± 1%	9 ± 3%
RGS4	86 ± 7%	0.0032 ± 0.0002%	36 ± 5%
FUS1-RGS4	78 ± 8%	0.0036 ± 0.0011%	45 ± 5%
P_{TET}-*SST2* (Dox = 0)	90 ± 8%	0.0059 ± 0.0023%	43 ± 2%
P_{TET}-*SST2* (Dox = 10 μg/ml)	60 ± 10%	0.16 ± 0.08%	39 ± 2%
P_{TET}-*RGS4* (Dox = 0)	76 ± 2%	0.19 ± 0.03%	43 ± 3%
P_{TET}-*RGS4* (Dox = 10 μg/ml)	18 ± 2%	10 ± 2%	10 ± 2%

*MAT*α tester strain was RJD357; the responder strains were *MAT**a***. In the mating discrimination assay, an RJD357 *mfα1*Δ *mfα2*Δ mutant strain was used as the pheromoneless decoy. In mating competition experiments, we determined the percent of diploids that resulted from mating with the responder strain instead of a wild-type competitor. The *MAT**a*** cells were $BAR1^+$ in these mating experiments. The data represent the mean ± SE ($n = 3$). Selected pairs of mating discrimination values were compared using a one-sided *t*-test, as described in the text. ND, not determined.

The *RGS4* strain had a slightly reduced mating efficiency (86%) compared to the wild-type *SST2* strain. There was also a 2.5-fold decrease in mating discrimination, and in the mating competition assay, 36% of the diploids were formed with the *RGS4* strain compared to 64% with the wild-type challenger. Together, these results show a modest but significant effect on mating proficiency by the replacement of *SST2* with *RGS4*.

The P_{TET}-*SST2* strain, when induced, displayed good mating efficiency (90%), but mating discrimination was fivefold lower than in the wild-type and the mating competition value was 43%. Optimal mating performance may be sensitive to slight changes in the transcription levels and regulation of the *SST2* gene. In the repressed state, the mating efficiency dropped to 60%, the mating discrimination was ~100-fold decreased from wild-type, and the mating competition value was 39%. This respectable level of mating performance was somewhat surprising given that the repressed strain was almost as supersensitive as the *sst2*Δ strain, which displayed more profound mating defects, arguing that at least some Sst2 is much better than none.

Finally, the P_{TET}-*RGS4* strain in the induced state had a mating competition value of 43%, but mating efficiency was relatively low (76%) and there was a 100-fold decrease in mating discrimination. These data indicated significant mating problems despite having pheromone sensitivity comparable to that of wild-type. In the repressed state, the strain exhibited mating defects of a magnitude similar to

that found for the *sst2*Δ strain. Even when repressed, the P_{TET}-*SST2* strain showed significantly better mating than the *sst2*Δ or repressed P_{TET}-*RGS4* strains. Our interpretation is that a small amount of Sst2, but not RGS4, can significantly improve mating compared to the complete absence of Sst2.

Focusing on the mating discrimination data, and starting with the wild-type strain, eliminating either transcriptional regulation (P_{TET}-*SST2*, induced) or protein regulation (P_{SST2}-*RGS4*) resulted in a three- to fivefold decline in discrimination, and each decrease was statistically significant (*t*-test) with $P < 0.05$ for P_{TET}-*SST2* and $P < 0.01$ for P_{SST2}-*RGS4*. However, removing both levels of regulation led to a more dramatic 100-fold decrease (P_{TET}-*RGS4*), $P < 0.001$.

Abnormal pheromone-induced morphologies in RGS variants

Wild-type cells treated with high concentrations of α-factor form multiple mating projections in a periodic pattern with a new projection appearing approximately every 2 h. As a positive control, we incubated unsynchronized wild-type cells with 1 μM α-factor and monitored projection formation as a function of time for 6 h (Fig. 2 *A*). After 2 h, *SST2*$^+$ cells contained ~0.5 projections/cell; after 4 h, 58% of the cells had formed the second projection; and after 6 h, wild-type *SST2* cells had an average of 2.6 mating projections (Table 2). The *sst2*Δ cells did not form multiple projections; they formed a relatively normal looking projection after 2 h, but no additional projections appeared over time, and instead the initial projection grew larger and broader.

The *RGS4* cells exhibited significant morphological defects at 1 μM α-factor. First, they also formed only a single projection, but compared to *sst2*Δ cells, the projection was more bent and irregular, possessing an amoeboid-like appearance. Furthermore, after 4 h, this projection often budded, resulting in a projection-budding (P&B) phenotype. From a temporal perspective, after 2 h, the RGS4 projection looked relatively normal. Indeed, at the 2-h time point, *SST2*, *sst2*Δ, and *RGS4* cells all had an average of 0.5 mating projections and were similar in appearance at a superficial level. Between 2 and 4 h, this projection in *RGS4* cells became bent and irregular, and between 4 and 6 h, many of these projections budded so that at 6 h, 74% of cells showed the P&B phenotype.

We investigated whether the RGS4 morphological phenotypes (single, bent projections that budded) were dominant. We expressed Sst2 from a single-copy plasmid in the *RGS4* strain and observed the morphology at $t = 6$ h (Fig. 2 *B*). It is of interest that most cells formed a second projection that budded. The same result was observed when RGS4 was expressed in wild-type *SST2*$^+$ cells. From this experiment, we concluded that the presence of Sst2 can cause a second projection to form, but the presence of RGS4 was a dominant gain-of-function alteration that caused the projection to bud.

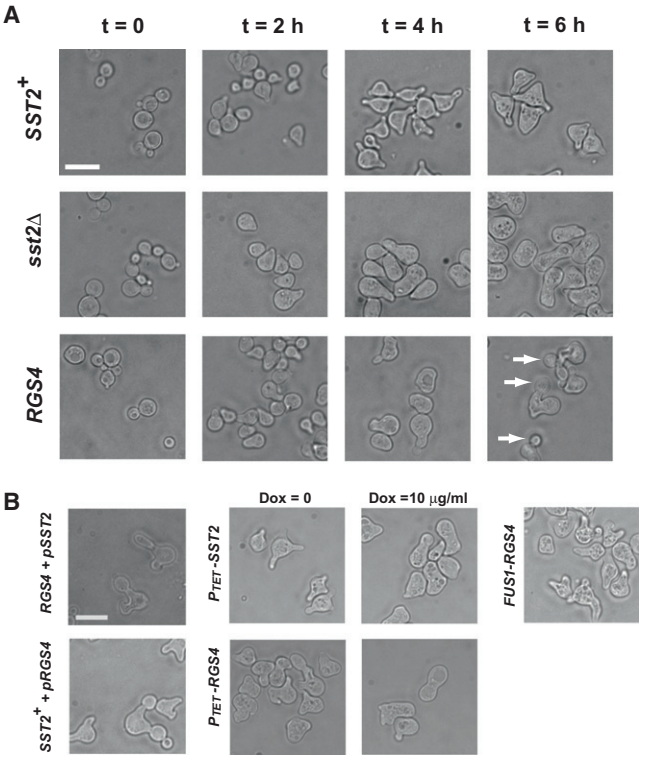

FIGURE 2 Morphological phenotypes of strains. (*A*) Time course of mating projection formation in *SST2*$^+$, *sst2*Δ, and *RGS4* strains. Each of the strains was treated with 1 μM α-factor for 0, 2, 4, and 6 h. The projection morphologies were assessed by bright-field imaging. Whereas the wild-type strain made multiple projections over time, the *sst2*Δ and *RGS4* strains made a single projection. In the *RGS4* cells, the projections were often crooked and budded from 4 to 6 h; buds emerging from the projections can be observed at the 6-h time point (*arrows*). Scale bar, 10 μm. (*B*) Morphological phenotypes for RGS variants containing Sst2 or RGS4. Cells were treated with 1 μM α-factor for 6 h. (*Upper left*) *RGS4* strain containing *SST2* on a single-copy plasmid. (*Lower left*) Wild-type strain containing *RGS4* on a single-copy plasmid. Both types of cells made more than one projection and showed projection-budding. (*Upper middle*) P_{TET}-*SST2* strain with 0 (induced) and 10 (repressed) μg/ml doxycyline. (*Lower middle*) P_{TET}-*RGS4* strain with 0 and 10 μg/ml doxycycline. (*Right*) Strain containing *RGS4* fused to the C-terminus of the *FUS1* gene.

TABLE 2 Average number of projections at $t = 6$ h

Strain	Number of projections
SST2$^+$	2.6
*sst2*Δ	1.0
RGS4	1.0
FUS1-RGS4	1.8
RGS4 + *pSST2*	1.5
SST2$^+$ + *pRGS4*	1.6
P_{TET}-*SST2* (Dox = 0)	2.4
P_{TET}-*SST2* (Dox = 0.1 μg/ml)	1.6
P_{TET}-*SST2* (Dox = 10 μg/ml)	1.0
P_{TET}-*RGS4* (Dox = 0)	1.0
P_{TET}-*RGS4* (Dox = 10 μg/ml)	1.0

In certain cases, the misshapen morphologies of the *RGS4* cells made it difficult to count the number of projections. We used time-lapse imaging on the *RGS4* strain to confirm the results in Table 2. The time-lapse data (Fig. S2) was consistent with the data on number of projections from the fixed cells, and the image sequence illustrates how these unusual morphologies can arise.

Effect of transcriptional regulation of *SST2* on pheromone-induced morphologies

We also substituted the P_{TET} promoter for the P_{SST2} promoter to examine the effect of transcriptional regulation on morphology. For example, one hypothesis is that pheromone induction of the *SST2* promoter is necessary for periodic projection formation through some negative feedback mechanism. To investigate such a possibility, we observed the P_{TET}-*SST2* cells at $t = 6$ h. It is interesting to note that in the absence of doxycyline (Sst2-expressed), P_{TET}-*SST2* cells formed multiple projections normally (Fig. 2 *B*) and the average number of projections (2.4) was almost the same as in wild-type *SST2* cells (Table 2). This result indicates that the native *SST2* promoter was not needed to form multiple projections. In the presence of doxycycline (Sst2-repressed), P_{TET}-*SST2* cells behaved like *sst2*Δ cells and formed a single projection. An intermediate morphological phenotype was observed with an intermediate dose of doxycycline (Table 2). Thus, the critical determinant of the number of mating projections was not the pheromone regulation of the promoter, but the dose of *SST2*.

We also examined the morphology of P_{TET}-*RGS4* cells. As expected, when RGS4 was expressed, the cells resembled the P_{SST2}-*RGS4* strain (one crooked projection that budded). In the presence of doxycycline, the morphology was more similar to *sst2*Δ cells (a straighter but broad projection that did not bud; Fig. 2 *B*).

Finally, we investigated the posttranslational modification of Sst2, examining the morphology of $SST2^{S539A}$ cells, which cannot be phosphorylated by Fus3 (12). The mutant cells possessed the same number of projections as wild-type cells (Fig. S3 *A*).

Spatial localization of RGS4

Sst2 exhibited a predominantly cytoplasmic localization pattern (data not shown; Ballon et al. (16)), but it was also observed on the plasma membrane, and localized to the mating projection membrane during the pheromone response (16). The association with the membrane was mediated through an interaction with Ste2, which was necessary for Sst2 action. The receptor Ste2 possesses a polarized distribution in the projection. We tracked localization of RGS4 fused to mCherry (29), which was expressed from a multicopy plasmid. RGS4 is known to bind to the plasma membrane (19), but we also found that during the mating response it appeared to be preferentially excluded from the projection (78% of cells), localizing to the membrane of the cell body with especially strong staining on the neck between the projection and cell body (Fig. S4 *A*). Although there was cell-to-cell variability in the distribution of RGS4, threshold analysis of the images demonstrated that on average, RGS4 localization was more prevalent in the cell body. We reasoned that this difference in the spatial patterning of Sst2 versus RGS4 contributed to the differences in morphology.

To test this hypothesis, we targeted RGS4 to the projection membrane by attaching RGS4 to Fus1. Fus1 is known to localize to the mating projection (30). By halo assay, the Fus1-RGS4 construct (26.5-mm halo) had roughly the same overall level of G-protein deactivation as the RGS4 strain (26-mm halo). Imaging of a Fus1-RGS4-mCherry protein demonstrated stronger localization at the projection and neck with weaker localization in the cell body (77% of cells; Fig. S4 *A*). Forced projection targeting of RGS4 partially complemented the morphological phenotype of *sst2*Δ cells, with most *FUS1-RGS4* cells forming a second projection (Table 2; 1.8 projections), and no projection budding observed.

However, the *FUS1-RGS4* strain did not exhibit improved mating performance over the *RGS4* strain (Table 1). One explanation is that most mating has occurred within the first 2 h, a time period in which the mating projection in the RGS4 strain is relatively normal. Thus, more proper spatial localization of the RGS functionality is able to partially correct the severe morphology phenotype of the RGS4 strain (a later phenotype), but not the more subtle mating impairment (earlier time points).

To investigate further the role of the localization of RGS proteins, we constructed the N^{RGS4}-*SST2* strain, in which the N-terminal helix of RGS4, which attaches to the membrane, was fused to the N-terminus of Sst2. (Fig. S3 *A*). We reasoned that the N^{RGS4} domain and the Sst2 DEP domain would compete for the localization of Sst2. Indeed, we observed a greater number of cells possessing a single projection (because of the influence of N^{RGS4}) compared to the wild-type, and the average number of projections decreased to 1.7 from 2.6. Conversely, we also constructed and examined the *MPI-RGS4* and *MPI-NΔRGS4* strains (Fig. S3 *B*), in which the MPI domain of Sst2 was attached to the N-terminus of either RGS4 or NΔRGS4 (RGS4 without the N-terminal membrane-attachment helix). Although these strains did not make multiple projections (perhaps because the MPI domain was not completely sufficient for proper localization), other aspects of the RGS4 phenotype, e.g., bending and projection-budding, were reduced (Fig. S3 *B*). Together, these results are consistent with the Fus1-RGS4 data on how localization domains of RGS proteins can influence yeast mating morphology.

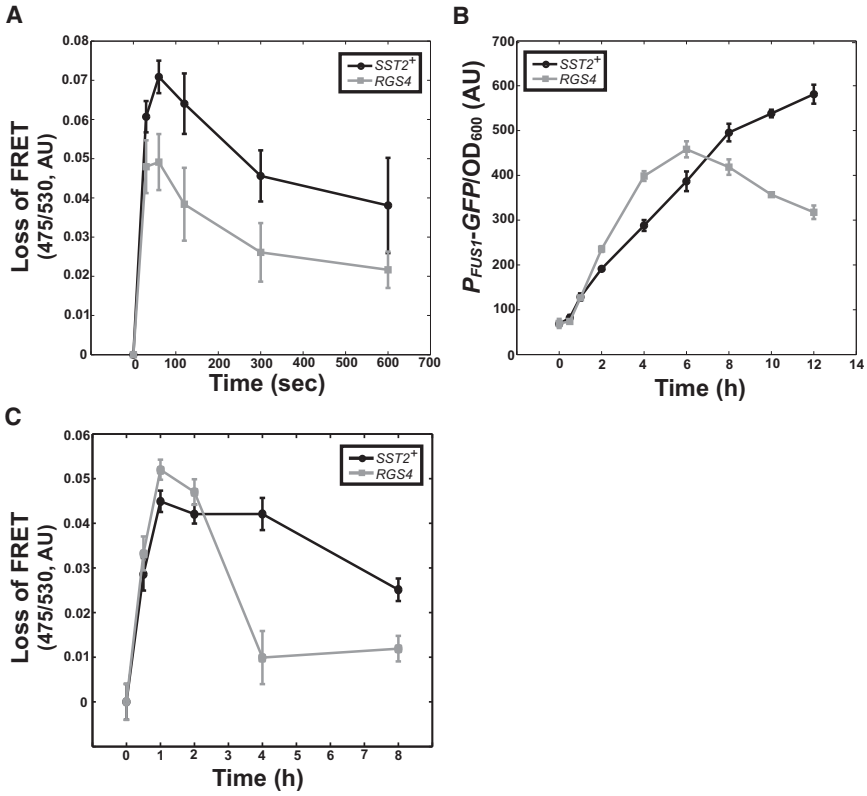

FIGURE 3 Time course of pheromone-induced G-protein and transcriptional activation in *RGS4* and $SST2^+$ strains. (*A*) Early G-protein activation in $SST2^+$ (*black*) and *RGS4* (*gray*) cells measured by loss of FRET. The FRET emission ratios (475/530 nm, arbitrary units) were measured at different time points from 0 to 10 min. These ratios were normalized by subtracting the $t = 0$ baseline. (*B*) Pheromone-induced transcription monitored by an integrated P_{FUS1}-*GFP* reporter; GFP fluorescence values (arbitrary units) were normalized to cell density (mean ± SE, $n = 3$). (*C*) Late G-protein activation in $SST2^+$ and *RGS4* cells (in P_{TET}-*STE2* background, 0 μg/ml doxycycline) measured by loss of FRET. The FRET emission ratios (475/530 nm, arbitrary units) were measured at different time points: $t = 0$, 0.5, 1, 2, 4, and 8 h. These ratios were normalized by subtracting the $t = 0$ baseline.

The dynamics of pheromone response in the *RGS4* strain

We treated cells possessing either *RGS4* or $SST2^+$ with 1 μM α-factor and recorded the time course of the response using two different reporter systems: 1), a strain containing the heterotrimeric G-protein-activation FRET reporters CFP-Gpa1 and Ste18-YFP; and 2), a strain containing the pheromone-responsive transcriptional reporter P_{FUS1}-*GFP*. Both reporters were integrated. The FRET reporter monitored early G-protein activation (first 10 min), whereas the GFP reporter monitored events (i.e., transcriptional induction) from 30 min to 8 h later.

As demonstrated in earlier work (1), the wild-type strain showed fast G-protein activation within 30 s, followed by a decrease. It is interesting that in the RGS4 strain, the peak amplitude was significantly lower than in the wild-type strain (Fig. 3 *A*). These data suggest that at early time points, RGS4 produced greater G-protein deactivation than did Sst2.

The dynamics of pheromone-induced transcription told a different story. In the wild-type *SST2* strain, pheromone-induced transcription increased continuously during the measured time points (Fig. 3 *B*). On the other hand, in the *RGS4* strain, there was an initial lag in GFP fluorescence compared to wild-type, but it increased faster starting at 2 h, and rose above the wild-type. It peaked at $t = 6$ h and then underwent a decline. The period of increase corresponded to when the wild-type cells were making a second projection, whereas the *RGS4* strain made only a single projection; the decrease corresponded to a period when the *RGS4* cells started to bud. We also monitored later time points of G-protein activation. G-protein activation levels in the *RGS4* strain were greater than that in the $SST2^+$ strain at $t = 1$ and 2 h (Fig. 3 *C*), but then decreased dramatically at $t = 4$ h. The observed faster increase followed by decrease in the *RGS4* strain was consistent with the P_{FUS1}-*GFP* transcription data. The fact that the decline occurred earlier in the FRET experiments presumably reflects the stability of enhanced GFP ($t_{1/2} \sim 7$ h) as well as the persistence of the signaling dynamics downstream of the G-protein.

Taken together these results indicate that RGS4 exerts a strong deactivation function early, when the cells are unpolarized, but that this deactivation decreases at later times, when the cell becomes more polarized. Then there is a sudden decline that correlates with budding.

Gradient sensing and morphological dose response of *RGS4* cells

We used microfluidics to explore the response of *RGS4* cells to a spatial gradient of α-factor, observing the ability to sense the gradient direction as well as the morphology at different doses. In the previous experiments, we treated cells

with 1 μM α-factor; the cells in the microfluidics chamber were exposed to a 0- to 100-nM gradient for 5 h (cells were *bar1*Δ). At the low concentrations, the RGS4 cells formed a relatively normal projection compared to wild-type cells (Fig. S4 *C*). At intermediate concentrations, some cells showed a sharply curved morphology not found in wild-type cells, which overall possessed a straighter projection. At the high end of the gradient, we observed the crooked, malformed RGS4 projections described in the 1-μM test tube experiments, whereas many wild-type cells formed a second projection. Thus, the *RGS4* strain formed curved projections that at higher α-factor concentrations became more irregular.

For both strains, cells in the low-dose range (~5–30 nM) possessed the most accurate projections, and we determined the directional accuracy for cells in this region of the chamber. Projection accuracy was measured as the cos(Θ) of the projection direction relative to the gradient direction (25). Wild-type cells showed an accuracy of 0.51 $\pm$ 0.10; the RGS4 cells showed a slightly lower projection accuracy of 0.36 $\pm$ 0.07. These data are consistent with the reduced mating performance of the *RGS4* strain.

Modeling spatial dynamics of G-protein activity and oscillations using a two-compartment model

The experimental data suggest that excess G-protein activation in the projection occurs in the *RGS4* cells and that this imbalance is responsible for the observed phenotypes. We wished to explore more quantitatively the connection between misregulated G-protein deactivation and the altered time-course data, the defects in mating and directional sensing, and the inability to make multiple projections. Previous work on modeling this system has primarily relied on nonspatial models (1–3,22,31,32); the few spatial models of the yeast pheromone response have focused more on cell polarity than on cell signaling (33,34). Because of the tight interconnection between signaling and polarization, we developed a hybrid model containing mechanistic G-protein equations and a generic representation of the polarity module (33) in a two-compartment model. The compartment containing the higher value of the polarity variable a_i, $i\in\{1, 2\}$, represents the projection, i.e., the compartment where polarized growth is occurring, and the other compartment represents the cell body. We approximated the two compartments to be of equal size (Fig. 4 *A*).

The equations of the heterotrimeric G-protein part of the model (Eqs. 1.1–1.6) are derived from previous time-course data of G-protein activation (1). The polarity part of the model (Eqs. 1.9 and 1.10) is a generic representation (33) intended to hide the details of the system in a few lumped parameters (k_1, h) that tune the positive feedback. One can think of the polarity variables a_1 and a_2 as corresponding loosely to active Cdc42 in the two compartments:

$$\frac{d[\mathrm{R_i}]}{dt} = -k_{RL}[\mathrm{L_i}][\mathrm{R_i}] + k_{RLm}[\mathrm{RL_i}] - k_{Rd\,0}[\mathrm{R_i}] + k_{Rs\,0} + P_{si}k_{Rs1} \tag{1.1}$$

$$\frac{d[\mathrm{RL_i}]}{dt} = k_{RL}[\mathrm{L_i}][\mathrm{R_i}] - k_{RLm}[\mathrm{RL_i}] - k_{Rd1}[\mathrm{RL_i}] \tag{1.2}$$

$$\frac{d[\mathrm{Ga_i}]}{dt} = k_{Ga}[\mathrm{RL_i}][\mathrm{G_i}] - k_{Gd}[\mathrm{Ga_i}] - k_{Gds}[\mathrm{Sst2_i}][\mathrm{Ga_i}] \tag{1.3}$$

$$\frac{d[\mathrm{Gbg_i}]}{dt} = k_{Ga}[\mathrm{RL_i}][\mathrm{G_i}] - k_{G1}[\mathrm{Gd_i}][\mathrm{Gbg_i}] \tag{1.4}$$

$$\frac{d[\mathrm{Gd_i}]}{dt} = k_{Gd}[\mathrm{Ga_i}] + k_{Gds}[\mathrm{Sst2_i}][\mathrm{Ga_i}] - k_{G1}[\mathrm{Gd_i}][\mathrm{Gbg_i}] \tag{1.5}$$

$$\frac{d[\mathrm{G_i}]}{dt} = k_{G1}[\mathrm{Gd_i}][\mathrm{Gbg_i}] - k_{Ga}[\mathrm{RL_i}][\mathrm{G_i}] \tag{1.6}$$

$$\frac{d[\mathrm{Sst2_i}]}{dt} = k_{Ssts\,0} + k_{Ssts\,0}[\mathrm{St12}] - k_{Sstd}[\mathrm{Sst2_i}] + k_T\frac{R_{ti}[\mathrm{Sst2_j}]}{\overline{R}_t} - k_T\frac{R_{tj}[\mathrm{Sst2_i}]}{\overline{R}_t} \tag{1.7}$$

$$\frac{d[\mathrm{St12}]}{dt} = k_{S12s}(Gbgn) - k_{S12d}[\mathrm{St12}] \tag{1.8}$$

$$\frac{da_i}{dt} = \frac{k_0}{1 + (Bgn_i)^{-q}} + \frac{k_1}{1 + (a_ip_i)^{-h}} - (k_2 + k_3b)a_i - k_5(\overline{a} - a_{ss})a_i + k_{cue} \tag{1.9}$$

$$\frac{db}{dt} = k_4(\overline{a} - a_{ss})b \tag{1.10}$$

$$i = 1, 2(\text{compartment } 1 \text{ or } 2),\ j = 2, 1$$

The connection between the two parts of the model occurs through two avenues. First, G$\beta\gamma$ is the output of the heterotrimeric G-protein cycle and the input to the polarity equations (Bgn_i=2[$\mathrm{Gbg_i}$]/[$\mathrm{Gbg_i}$]+[$\mathrm{Gbg_j}$]), reflecting its key role in determining the location of polarization (35). Second, receptor and other components of this system are directed to the projection ($P_{si} = 2a_i/a_i+a_j$) according to the polarity variable a_i (36).

The polarized distribution of Sst2 depends on the concentration of total receptor in each compartment and is implemented by the transport terms (k_T). In the RGS4 model, the RGS4 localization is the reverse of the typical localization of Sst2 in a wild-type cell,with a greater concentration of RGS4 on the cell body membrane than on the projection membrane. More details about the model are available in the Supporting Material.

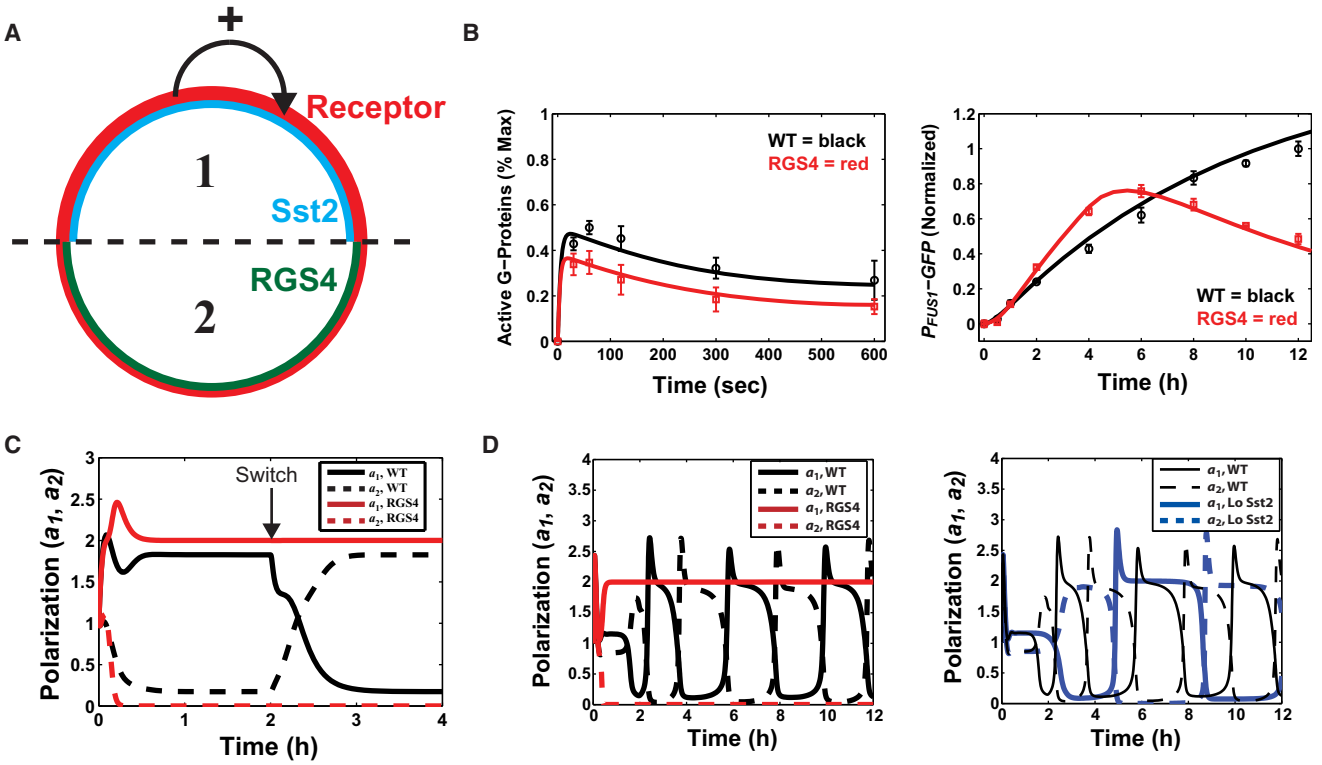

FIGURE 4 Mathematical modeling of heterotrimeric G-protein signaling and projection formation using a two-compartment model. (*A*) Two-compartment model of cell signaling. One compartment represents the projection and the other the cell body; these identities depend on value of the polarization variables a_1 and a_2 (high = projection, low = cell body). The compartments are considered to be of equal size. The polarization module reads the active G-protein gradient and amplifies it. Receptor localization (*red*) depends on this polarization feeding back on receptor synthesis in a positive feedback loop. Sst2 is preferentially distributed in the projection (*blue*), whereas RGS4 (*green*) is primarily found in the cell body. (*B*) Fitting the model to the G-protein FRET data (*left*) and P_{FUS1}-*GFP* data (*right*). Data points are from Fig. 3; wild-type (*black*) and RGS4 (*red*) simulations are shown. The peak of the wild-type G-protein activation was assigned a fractional value of 50%, as previously estimated (1). For the transcription data, the P_{FUS1}-*GFP* values were normalized to the 12-h time point for wild-type. (*C*) Simulations of wild-type cells (*black*) can track the gradient change, but simulations of *RGS4* cells (*red*) cannot. The polarization variables a_1 and a_2 are plotted versus time. The initial α-factor concentration was 11 nM in compartment 1 and 9 nM in compartment 2, and this gradient was switched at $t = 2$ h. (*D*) Oscillations produced by the model with negative feedback. Adding a negative feedback loop resulted in a model that oscillates for wild-type parameters (*black*). The RGS4 model is stuck in the initial polarization direction and does not oscillate (*left*, *red*). Reducing the Sst2-catalyzed deactivation activity 10-fold resulted in a longer periodicity (*right*, *blue*) for the oscillations, reflecting the fewer projections produced by cells possessing a lower level of Sst2. Ligand concentration was 1 μM in both compartments.

One unexpected feature of the time-course data is that the *RGS4* strain exhibited reduced G-protein activation during the early response (first 10 min), but after 1 h showed increased transcription of the P_{FUS1}-*GFP* reporter compared to the wild-type strain. We modeled that Sst2 was polarized to the mating projection through binding to the Ste2 receptor (16), whereas RGS4 was antipolarized to the cell body, as observed in our data (Fig. 4 *A*). There was a positive feedback loop in which greater G-protein activity in the projection was amplified by the polarization module leading to polarized synthesis of new receptors to the projection (34,36). We derived a kinetic rate constant for RGS4 G-protein deactivation by fitting the nominal model to the RGS4 curve, allowing only the G-protein deactivation rate constant (k_{Gds4}) to vary, which was 1.6-fold greater than the wild-type. We then fit the transcription time-course data by adjusting the kinetic rate constant for the production of GFP, which also contained an exponential decay term to GFP synthesis, to represent the budding after 4 h; the half-life of GFP was set at 7 h (37). The good fit indicated that the localization model was consistent with the time-course data (Fig. 4 *B*).

A second issue addressed with the modeling was the defect in *RGS4* cells in the mating assays and in sensing the gradient direction. Accurate gradient sensing and mating requires continuous sensing, because the source may be moving or the initial projection direction may be incorrect. Excess G-protein activity can feed the polarization positive feedback loop, resulting in hysteresis (arising from bistability) and irreversible projection growth; the polarized distribution of Sst2 bound to receptor can counterbalance this positive feedback, preventing this irreversible projection.

In the simulations, we applied the gradient in one direction and then switched the direction 180°. Simulated wild-type cells were able to track this directional change (Fig. 4 *C*, *black lines*) and flip the polarization so that

$a_2 > a_1$. On the other hand, the simulated *RGS4* cells maintained the polarization with $a_1 > a_2$, despite the change in the gradient. In the RGS4 simulations, positive feedback caused the polarization to become stuck in the initial direction when the gradient direction was flipped. There are two positive feedback loops. The first is in the polarization module and results in the polarization of species *a*. The second is the polarized synthesis of the receptor. Both are necessary and depend on the level and distribution of active G-protein. The polarized localization of Sst2 counteracts the polarized synthesis of receptor by enhancing deactivation of G-protein where activation is strong. In the RGS4 cells, the deactivation is not heightened in the projection, and so the positive feedback maintains the polarization despite the change in gradient direction.

Finally, we modeled the formation of multiple projections. We attempted to capture the spatial nature of the oscillations in which the polarity would shift from one compartment to the other. To obtain the oscillations, we added a delayed negative feedback to the model, which inhibited G-protein activation (Supporting Material). We chose a generic formulation of this feedback because the exact mechanism is not known. By tuning the feedback gain, we obtained oscillations for the wild-type model with a period of ~2 h (21). The wild-type simulations showed the oscillations, but the *RGS4* simulations did not. Instead, the *RGS4* polarization became stuck and could not oscillate because of the irreversible projection growth (Fig. 4 *D*, *left*). Our experimental data demonstrated that an intermediate level of Sst2 (expressed from the partially induced P_{TET} promoter) produced fewer projections, and indeed, in the simulations, 10-fold-reduced Sst2 activity increased the period of the oscillations by approximately twofold (Fig. 4 *D*, *right*, *blue lines*). Thus, we were able to capture the essential spatial dynamics of this system with a low-order model and a coarse spatial description, which highlighted the importance of the spatial aspect of G-protein signaling, and the importance of the polarized localization of Sst2 to balance the amplified activation of G-protein.

DISCUSSION

In this study, we investigated the role of regulation of the RGS protein on the yeast mating response, a canonical G-protein system, by replacing the *SST2* gene with the heterologous P_{TET} promoter and the human *RGS4* coding region. Our results suggest that fine-tuning in both space and time of the amount of G-protein activity by Sst2 is important for optimal mating behavior. Many of the RGS variants, including the P_{TET}-*RGS4* strain, possessed normal pheromone sensitivity assessed by the halo assay, and yet they displayed significant defects in morphogenesis and mating. More generally, the combination of experiments and modeling support the general conclusions that the spatial dynamics of RGS proteins are important for proper cell polarity, that too much G-protein signaling in a certain location (e.g., projection) can produce abnormal cell morphologies, and that the spatial dynamics of G-protein regulators play an important role in the oscillatory behavior of G-protein systems. As a result, it is important to link the spatial dynamics of activator (GPCR) and deactivator (RGS).

Ballon et al. (16) demonstrated that the DEP domain in the N-terminal region of Sst2 binds to the Ste2 receptor and that this interaction is necessary to bring Sst2 to the plasma membrane, where it functions. We have built upon these observations, showing that this polarized localization is likely to play a role in formation of multiple projections. Localization of RGS4 at the membrane was enough to complement the supersensitive phenotype of *sst2*Δ cells, but in the absence of this polarization, it was not enough to complement the morphological phenotype of *sst2*Δ cells. Forced targeting of RGS4 to the projection (*FUS1-RGS4*) was needed to produce multiple projections.

We believe that the projection-budding phenotype in *RGS4* cells was caused by the nonpolarized localization of RGS4. In wild-type cells, we hypothesize that negative feedback suppresses G-protein signaling in the projection, but the relative absence of Sst2 on the cell body membrane allows the initiation of a second projection. On the other hand, RGS4, with its preferential localization on the cell body membrane, prevents formation of a second projection, and over time, negative feedback of G-protein signaling in the first projection downregulates signaling, eventually resulting in resumption of the cell cycle and budding.

There has been extensive modeling of the mating response in yeast (e.g., (2,22,34,38). Here we have linked the heterotrimeric G-protein cycle with aspects of cell polarity in a two-compartment spatial model. Simulations of the model, which contained some fitted parameters, offered one possible explanation for the time-course data by demonstrating that the mislocalization RGS4 can cause increased P_{FUS1}-*GFP* expression compared to wild-type at later time points. In addition, the modeling showed that gradient-sensing and response could be disrupted by excessive G-protein signaling in the projection caused by the absence of RGS4 in this compartment. Finally, we constructed an oscillator that combined positive feedback by the polarity module and by receptor polarization with negative feedback acting on the G-protein cycle. Reducing the level of Sst2 increased the period, and adding RGS4 prevented oscillations, as observed in experiments (Fig. 4 *D*). Together, the simulations demonstrate that linking Sst2 to receptor helps to fine-tune the spatial dynamics of G-protein signaling, which is important for optimal performance of mating and projection formation.

In the model, we implemented specific terms whose accuracy requires further validation. For example, the localization terms of Sst2 and RGS4 are based on the data of

Ballon et al., as well as on our own observations, but quantitative confirmation would be important. In addition, we proposed a negative feedback loop in a very generic fashion. One hypothesis is that receptor downregulation by receptor hyperphosphorylation may contribute to this feedback. One can test this hypothesis by disrupting receptor downregulation and examining the effect on the formation of multiple projections. More generally, it is a priority to replace the phenomenological constraints in the model with experimentally supported mechanistic terms, and to check the validity of the assumptions (e.g., time-delay negative feedback). It should be noted that we do not preclude the possibility that the additional negative feedback may act through Sst2, presumably through a posttranscriptional mechanism.

It is known that RGS proteins in other systems interact with GPCRs (39) for the same purpose: to ensure that the deactivator is in close proximity to the activator to create properly regulated spatial dynamics. A general attribute of signaling systems is that too much signaling can be just as detrimental as too little signaling (40). This work demonstrates that the spatial distributions of activator and deactivator of heterotrimeric G-protein signaling are important for cell morphology and polarity.

SUPPORTING MATERIAL

Additional explanations, descriptions, equations, tables, figures, and references are available at http://www.biophysj.org/biophysj/supplemental/S0006-3495(10)00664-8.

We thank all members of the Yi lab for helpful comments and suggestions.

This work was supported by National Institutes of Health grant P50GM76516 and R01GM75309.

REFERENCES

1. Yi, T. M., H. Kitano, and M. I. Simon. 2003. A quantitative characterization of the yeast heterotrimeric G protein cycle. *Proc. Natl. Acad. Sci. USA.* 100:10764–10769.
2. Hao, N., N. Yildirim, …, H. G. Dohlman. 2003. Regulators of G protein signaling and transient activation of signaling: experimental and computational analysis reveals negative and positive feedback controls on G protein activity. *J. Biol. Chem.* 278:46506–46515.
3. Kofahl, B., and E. Klipp. 2004. Modelling the dynamics of the yeast pheromone pathway. *Yeast.* 21:831–850.
4. Sprague, G. F. J., and J. W. Thorner. 1992. Pheromone response and signal transduction during the mating process of *Saccharomyces cerevisiae*. *In* The Molecular and Cellular Biology of the Yeast *Saccharomyces*: Gene Expression. Cold Spring Harbor Laboratory, Cold Spring Harbor, NY. 657–744.
5. Dohlman, H. G., and J. W. Thorner. 2001. Regulation of G protein-initiated signal transduction in yeast: paradigms and principles. *Annu. Rev. Biochem.* 70:703–754.
6. Hao, N., M. Behar, …, H. G. Dohlman. 2007. Systems biology analysis of G protein and MAP kinase signaling in yeast. *Oncogene.* 26:3254–3266.
7. Chan, R. K., and C. A. Otte. 1982. Isolation and genetic analysis of *Saccharomyces cerevisiae* mutants supersensitive to G1 arrest by **a** factor and α factor pheromones. *Mol. Cell. Biol.* 2:11–20.
8. Apanovitch, D. M., K. C. Slep, …, H. G. Dohlman. 1998. Sst2 is a GTPase-activating protein for Gpa1: purification and characterization of a cognate RGS-Gα protein pair in yeast. *Biochemistry.* 37: 4815–4822.
9. Jackson, C. L., and L. H. Hartwell. 1990. Courtship in *S. cerevisiae*: both cell types choose mating partners by responding to the strongest pheromone signal. *Cell.* 63:1039–1051.
10. Dohlman, H. G., J. Song, …, J. Thorner. 1996. Sst2, a negative regulator of pheromone signaling in the yeast *Saccharomyces cerevisiae*: expression, localization, and genetic interaction and physical association with Gpa1 (the G-protein α subunit). *Mol. Cell. Biol.* 16: 5194–5209.
11. Dietzel, C., and J. Kurjan. 1987. Pheromonal regulation and sequence of the *Saccharomyces cerevisiae* SST2 gene: a model for desensitization to pheromone. *Mol. Cell. Biol.* 7:4169–4177.
12. Garrison, T. R., Y. Zhang, …, H. G. Dohlman. 1999. Feedback phosphorylation of an RGS protein by MAP kinase in yeast. *J. Biol. Chem.* 274:36387–36391.
13. Parnell, S. C., L. A. Marotti, Jr., …, H. G. Dohlman. 2005. Phosphorylation of the RGS protein Sst2 by the MAP kinase Fus3 and use of Sst2 as a model to analyze determinants of substrate sequence specificity. *Biochemistry.* 44:8159–8166.
14. Hoffman, G. A., T. R. Garrison, and H. G. Dohlman. 2000. Endoproteolytic processing of Sst2, a multidomain regulator of G protein signaling in yeast. *J. Biol. Chem.* 275:37533–37541.
15. Xu, B. E., K. R. Skowronek, and J. Kurjan. 2001. The N terminus of *Saccharomyces cerevisiae* Sst2p plays an RGS-domain-independent, Mpt5p-dependent role in recovery from pheromone arrest. *Genetics.* 159:1559–1571.
16. Ballon, D. R., P. L. Flanary, …, J. Thorner. 2006. DEP-domain-mediated regulation of GPCR signaling responses. *Cell.* 126:1079–1093.
17. Druey, K. M., K. J. Blumer, …, J. H. Kehrl. 1996. Inhibition of G-protein-mediated MAP kinase activation by a new mammalian gene family. *Nature.* 379:742–746.
18. Chen, T., and J. Kurjan. 1997. *Saccharomyces cerevisiae* Mpt5p interacts with Sst2p and plays roles in pheromone sensitivity and recovery from pheromone arrest. *Mol. Cell. Biol.* 17:3429–3439.
19. Srinivasa, S. P., L. S. Bernstein, …, M. E. Linder. 1998. Plasma membrane localization is required for RGS4 function in *Saccharomyces cerevisiae*. *Proc. Natl. Acad. Sci. USA.* 95:5584–5589.
20. Bücking-Throm, E., W. Duntze, …, T. R. Manney. 1973. Reversible arrest of haploid yeast cells in the initiation of DNA synthesis by a diffusible sex factor. *Exp. Cell Res.* 76:99–110.
21. Bidlingmaier, S., and M. Snyder. 2004. Regulation of polarized growth initiation and termination cycles by the polarisome and Cdc42 regulators. *J. Cell Biol.* 164:207–218.
22. Hilioti, Z., W. Sabbagh, Jr., …, A. Levchenko. 2008. Oscillatory phosphorylation of yeast Fus3 MAP kinase controls periodic gene expression and morphogenesis. *Curr. Biol.* 18:1700–1706.
23. Guthrie, C., and G. R. Fink. 1991. Guide to Yeast Genetics and Molecular Biology. Academic Press, San Diego.
24. Hartwell, L. H. 1980. Mutants of *Saccharomyces cerevisiae* unresponsive to cell division control by polypeptide mating hormone. *J. Cell Biol.* 85:811–822.
25. Moore, T. I., C. S. Chou, …, T. M. Yi. 2008. Robust spatial sensing of mating pheromone gradients by yeast cells. *PLoS ONE.* 3:e3865.
26. Garí, E., L. Piedrafita, …, E. Herrero. 1997. A set of vectors with a tetracycline-regulatable promoter system for modulated gene expression in *Saccharomyces cerevisiae*. *Yeast.* 13:837–848.
27. Reference deleted in proof.
28. Jackson, C. L., J. B. Konopka, and L. H. Hartwell. 1991. *S. cerevisiae* α pheromone receptors activate a novel signal transduction pathway for mating partner discrimination. *Cell.* 67:389–402.
29. Shaner, N. C., R. E. Campbell, …, R. Y. Tsien. 2004. Improved monomeric red, orange and yellow fluorescent proteins derived from *Discosoma* sp. red fluorescent protein. *Nat. Biotechnol.* 22:1567–1572.

30. Proszynski, T. J., R. Klemm, …, K. Simons. 2006. Plasma membrane polarization during mating in yeast cells. *J. Cell Biol.* 173:861–866.

31. Wang, X., N. Hao, …, T. C. Elston. 2006. Bistability, stochasticity, and oscillations in the mitogen-activated protein kinase cascade. *Biophys. J.* 90:1961–1978.

32. Paliwal, S., P. A. Iglesias, …, A. Levchenko. 2007. MAPK-mediated bimodal gene expression and adaptive gradient sensing in yeast. *Nature.* 446:46–51.

33. Chou, C. -S., Q. Nie, and T. -M. Yi. 2008. Modeling robustness tradeoffs in yeast cell polarization induced by spatial gradients. *PLoS ONE.* 3:e3103.

34. Altschuler, S. J., S. B. Angenent, …, L. F. Wu. 2008. On the spontaneous emergence of cell polarity. *Nature.* 454:886–889.

35. Nern, A., and R. A. Arkowitz. 1998. A GTP-exchange factor required for cell orientation. *Nature.* 391:195–198.

36. Marco, E., R. Wedlich-Soldner, …, L. F. Wu. 2007. Endocytosis optimizes the dynamic localization of membrane proteins that regulate cortical polarity. *Cell.* 129:411–422.

37. Mateus, C., and S. V. Avery. 2000. Destabilized green fluorescent protein for monitoring dynamic changes in yeast gene expression with flow cytometry. *Yeast.* 16:1313–1323.

38. Behar, M., N. Hao, …, T. C. Elston. 2008. Dose-to-duration encoding and signaling beyond saturation in intracellular signaling networks. *PLOS Comput. Biol.* 4:e1000197.

39. Luo, X., S. Popov, …, S. Muallem. 2001. RGS proteins provide biochemical control of agonist-evoked $[Ca^{2+}]_i$ oscillations. *Mol. Cell.* 7:651–660.

40. Alberts, B., D. Bray, …, J. D. Watson. 1994. Molecular Biology of the Cell. Garland Press, New York.